

Motion Manifold Flow Primitives for Language-Guided Trajectory Generation

Yonghyeon Lee¹ Byeongho Lee² Seungyeon Kim² Frank C. Park²

¹ Korea Institute for Advanced Study (KIAS) ² Seoul National University
ylee@kias.re.kr {bhlee, ksy}@robotics.snu.ac.kr fcp@snu.ac.kr

Abstract: Developing text-based robot trajectory generation models is made particularly difficult by the small dataset size, high dimensionality of the trajectory space, and the inherent complexity of the text-conditional motion distribution. Recent manifold learning-based methods have partially addressed the dimensionality and dataset size issues, but struggle with the complex text-conditional distribution. In this paper we propose a text-based trajectory generation model that attempts to address all three challenges while relying on only a handful of demonstration trajectory data. Our key idea is to leverage recent flow-based models capable of capturing complex conditional distributions, not directly in the high-dimensional trajectory space, but rather in the low-dimensional latent coordinate space of the motion manifold, with deliberately designed regularization terms to ensure smoothness of motions and robustness to text variations. We show that our *Motion Manifold Flow Primitive (MMFP)* framework can accurately generate qualitatively distinct motions for a wide range of text inputs, significantly outperforming existing methods.

Keywords: LfD, movement primitives, manifold, flow-based models

1 Introduction

Past successes in text-based generative models for applications ranging from image synthesis [1, 2] and 3D scene construction [3, 4] to human motion generation [5, 6] can broadly be traced to two technical advancements: (i) large-scale pre-trained text embedding models based on transformer architectures [7, 8], and (ii) efficient training methods for probability density flow-based models that are capable of learning complex conditional density functions, e.g., diffusion [9, 10], score-based [11], and continuous normalizing flow models [12, 13, 14]. In this paper, we address the problem of generating a set of robot motions from a user-provided text instruction.

Most existing text-based generative models rely on extensive text-annotated data for training, ranging from tens of thousands to several billion pieces of data. In contrast, we assume only a handful of demonstration data is available, making training flow-based models in high-dimensional trajectory space particularly challenging. Specifically, a flow-based model must

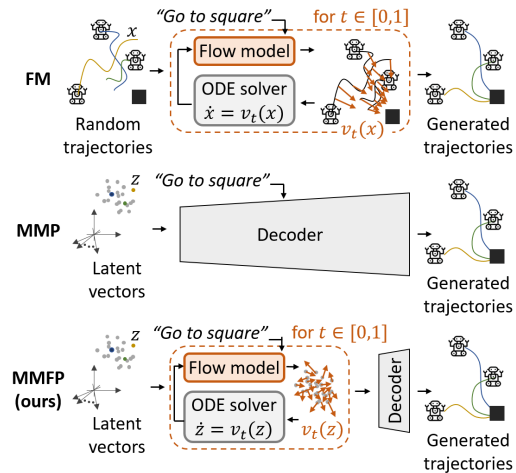


Figure 1: *Upper:* Flow-based Model (FM) in the trajectory space. *Middle:* Motion Manifold Primitives (MMP) with a single decoder. *Lower:* Motion Manifold Flow Primitives (MMFP), a flow-based model in the learned motion manifold.

learn a vector field that transforms the high-

dimensional Gaussian distribution to the distribution of the demonstration trajectory data, as illustrated in Figure 1 (*Upper*). Not surprisingly, having only a small number of demonstration trajectories leads to poor generation performance, as shown later in our experiments.

Instead, leveraging a low-dimensional manifold structure can be an effective solution. Assuming the set of demonstration trajectories lies on a lower-dimensional manifold embedded in the trajectory space (the manifold hypothesis), recent works such as Motion Manifold Primitives (MMP) [15] and Task-Conditional Variational Autoencoders (TCVAE) [16] exploit this structure. These methods use an autoencoder framework, where a decoder transforms a low-dimensional latent space distribution (e.g., Gaussian or Gaussian Mixture Model) to the task-conditional data distribution, given a task parameter. These models can be used by regarding texts as task parameters (Figure 1 *Middle*). However, text-conditional trajectory distributions are inherently complex, with varying numbers of modalities and volumes of support based on the input text. Our studies indicate that a single decoder network struggles to learn these complex conditional distributions.

In this paper we propose the *Motion Manifold Flow Primitive (MMFP)* framework, which combines the advantage of flow-based models capable of learning complex conditional distributions with motion manifold primitives capable of encoding and generating low-dimensional manifold of trajectories. Our proposed method consists of two steps. We first learn a decoder that parametrizes the motion manifold. In the low-dimensional latent coordinate space, we then train a flow-based model by using the recent flow matching algorithm of [12]. Specifically, we design proper regularization terms to ensure the smoothness of the generated trajectories and robustness against unstructured text variations that preserve meanings. As illustrated in Figure 1 (*Lower*), given a text, the latent flow-based model first transforms the low-dimensional latent Gaussian to the text-conditional latent space distribution, and then the decoder maps it to the trajectory space distribution.

We evaluate the performance of MMFP through two text-based trajectory generation tasks: (i) a bottle’s SE(3) trajectory generation for pouring task and (ii) a 7-DoF robot arm’s waving trajectory generation task. Notably, with only 10 and 30 demonstration trajectories for each respective task, MMFP shows excellent performance. In contrast, diffusion and flow-based models trained directly in the high-dimensional trajectory space [9, 12, 13] and existing motion manifold primitives-based methods [16, 15] fail to generate successful trajectories.

2 Related Works

2.1 Movement primitives

There are many studies on movement primitives, e.g., dynamic movement primitives [17, 18, 19, 20, 21, 22, 23, 24, 25, 26], stable dynamical systems [27, 28, 29, 30, 31, 32, 33, 34, 35], methods to represent diverse motions [36, 37, 38, 39, 40, 16, 15]. Of particular relevance to our problem is the task-conditional movement primitives capable of generating diverse trajectories that perform the given task. Text inputs can be transformed into text embedding vectors using pre-trained language models [7, 8], and these vectors can be treated as task parameters. Task-Parametrized Gaussian Mixture Model (TP-GMM) [36] is capable of generating new movements based on unseen task parameters. However, its emphasis is on a specific type of task parameters, such as frames of reference, making it unsuitable for handling text embedding vectors. Recent deep autoencoder-based methods such as Task-Conditional Variation Autoencoder (TCVAE) [16] and Motion Manifold Primitives (MMPs) [15] can take general types of task parameters. However, they show far less-than-desirable performance given the complexity of the text-conditional trajectory distribution.

2.2 Language-based generative models

Recent success of text-conditional deep generative models in image [1, 2, 41, 42, 43], human motion [5, 6, 44], and 3D scene generation tasks [3, 4] is not only attributed to transformer-based text embedding methods [7, 8, 45, 46, 47] and efficient training methods for flow-based conditional generative models [9, 10, 11, 12, 13, 14], but also relies heavily on the abundance of text-annotated train-

ing data. In contrast, text-based generation of robot arm motions has received relatively less attention, partly due to limited demonstration data. Notable exceptions include the open X-embodiment robot learning datasets [48] and generalist robotic transformers [49], which are trained using extensive text-annotated robot motion data. However, challenges persist in generating complex 6-DoF motions, confining their capabilities primarily to simpler actions like pick-and-place. Our objective sets us apart, as we aim to develop a language-based model that can generate complex 6-DoF motions for specific tasks, yet using a limited amount of demonstration data.

3 Preliminaries

3.1 Autoencoder-based manifold learning

In this section, we briefly introduce an autoencoder and its manifold learning perspective [50, 51, 52, 53, 54, 55, 56]. Consider a high-dimensional data space \mathcal{X} and a set of data points $\mathcal{D} = \{x_i \in \mathcal{X}\}_{i=1}^N$. We adopt the manifold hypothesis that the data points $\{x_i\}$ lie approximately on some lower-dimensional manifold \mathcal{M} in \mathcal{X} . Suppose \mathcal{M} is an m -dimensional manifold and let \mathcal{Z} be a latent space \mathbb{R}^m . An encoder is a mapping $g : \mathcal{X} \rightarrow \mathcal{Z}$ and a decoder is a mapping $f : \mathcal{Z} \rightarrow \mathcal{X}$. These are often approximated with deep neural networks and trained to minimize the reconstruction loss $\frac{1}{N} \sum_{i=1}^N d^2(f \circ g(x_i), x_i)$ given a distance metric $d(\cdot, \cdot)$ on \mathcal{X} . We note that, given a sufficiently low reconstruction error, all the data points $\{x_i\}$ should lie on the image of the decoder f . Under some mild conditions¹, the image of f is an m -dimensional differentiable manifold embedded in \mathcal{X} , i.e., the decoder produces a lower-dimensional manifold where the data points approximately lie.

3.2 Continuous normalizing flow and flow matching

In this section, we introduce the continuous normalizing flow [57] and its efficient training method, the flow matching algorithm [12]. Let $\{x_i \in \mathcal{X}\}_{i=1}^N$ be a set of data points sampled from the underlying probability density $q(x)$. Consider a time-dependant vector field $v : [0, 1] \times \mathcal{X} \rightarrow T\mathcal{X}$ that leads to a flow $\phi : [0, 1] \times \mathcal{X} \rightarrow \mathcal{X}$ via the following ordinary differential equation: $\frac{d}{dt} \phi_t(x) = v_t(\phi_t(x))$, where $\phi_0(x) = x$. Given a prior density at $t = 0$ denoted by p_0 , the flow ϕ_t leads to a probability density path for $t \in [0, 1]$ [12]: $p_t(x) = p_0(\phi_t^{-1}(x)) \det \left(\frac{\partial \phi_t^{-1}}{\partial x}(x) \right)$. Our objective is to learn a neural network model of $v_t(x)$ so that the flow of $v_t(x)$ transforms a simple prior density p_0 (e.g., Gaussian) to the target data distribution $p_1 \approx q$. Then we can sample new data points by solving the ODE from $t = 0$ to $t = 1$ with initial points sampled from p_0 .

The standard maximum log-likelihood training requires expensive numerical ODE simulations [57], instead we introduce an efficient simulation-free approach for training $v_t(x)$ [12]. In the first step, we design a conditional probability path $p_t(x|x_1)$ for $x_1 \sim q(x)$ such that $p_0(x|x_1) = p_0(x)$ and $p_1(x|x_1)$ is concentrated around $x = x_1$. For example, Lipman et al. [12] suggests an Optimal Transport (OT) Gaussian probability path $p_t(x|x_1) = \mathcal{N}(x|x_1, (1 - (1 - \sigma_{min})t)^2 I)$ where σ_{min} is set to be small. Theorem 3 in [12] states that $u_t(x|x_1) = \frac{x_1 - (1 - \sigma_{min})x}{1 - (1 - \sigma_{min})t}$ generates the Gaussian path $p_t(x|x_1)$. Then, Lipman et al. [12] shows that minimizing the following flow matching objective function $\mathbb{E}_{x_1 \sim q(x), t \sim \mathcal{U}[0,1], x \sim p_t(x|x_1)} [\|v_t(x) - u_t(x|x_1)\|^2]$, where $\mathcal{U}[0, 1]$ is the uniform distribution between 0 and 1, leads to a vector field $v_t(x)$ generating $p_1(x) = \int p_1(x|x_1)q(x_1)dx_1$ which closely approximates the data distribution q .

Our particular interest is a conditional density function $p(x|c)$ for a condition variable c (e.g., text) which requires slight modifications. We model a neural network vector field $v_t(x, c)$ that takes an additional input c . Then, we minimize the following objective function:

$$\mathbb{E}_{(x_1, c) \sim q(x, c), t \sim \mathcal{U}[0,1], x \sim p_t(x|x_1)} [\|v_t(x, c) - u_t(x|x_1)\|^2], \quad (1)$$

where $q(x, c)$ is the underlying joint data distribution. In practice, sampling from $q(x, c)$ is replaced by sampling from the dataset $\{(x_i, c_i)\}_{i=1}^N$.

¹ m is lower than the dimension of the data space \mathcal{X} and f is smooth and its Jacobian $\frac{\partial f}{\partial z}(z) \in \mathbb{R}^{\dim(\mathcal{X}) \times m}$ is full rank everywhere.

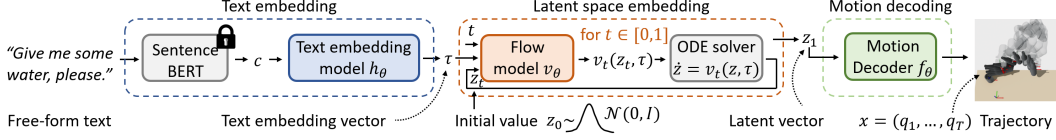


Figure 2: The procedure of motion generation in MMFP: (i) the Sentence-BERT encodes a free-form text into a vector c , (ii) the text embedding model h_θ maps c to a text embedding vector τ , (iii) we solve the ODE $\dot{z} = v_t(z, \tau; \theta)$ from $t = 0$ to $t = 1$ with an initial value z_0 sampled from Gaussian $\mathcal{N}(z|0, I)$ and obtain $z_1 \in \mathcal{Z}$, and (iv) the motion decoder f_θ maps z_1 to a trajectory $x = (q_1, \dots, q_T)$.

4 Language-based Robot Motion Generation

We begin this section with some notations. Let \mathcal{Q} be a configuration space. Denote a sequence of configurations by $x = (q_1, \dots, q_T)$, called a trajectory, for $q_i \in \mathcal{Q}$ and some positive integer $T > 0$. The number of configurations T is fixed throughout. We assume that the time interval between q_i and q_{i+1} is constant as dt , so the total time is $(T - 1) \times dt$. We will denote the trajectory space by $\mathcal{X} = \mathcal{Q}^T$. We use a pre-trained text encoder, the Sentence-BERT [58], without fine-tuning and it encodes free-form texts into 768-dimensional vectors; these encoded vectors are denoted by c . We assume that we are provided with a set of demonstration trajectories, each of which is annotated with M different texts, i.e., the dataset is $\mathcal{D} = \{(x_i, \{c_{ij}\}_{j=1}^M)\}_{i=1}^N$ for $x_i \in \mathcal{X}$ and $c_{ij} \in \mathbb{R}^{768}$. We will use the same symbol θ to represent the learnable parameters of different neural networks with a slight abuse of notation, and denote a parametric neural network function by $f_\theta(x)$ or $f(x; \theta)$.

The overall framework of our method is shown in Figure 2. Our framework consists of two modules: (i) motion manifold model and (ii) latent space flow-based models. Below, we describe how to train each module.

Smooth motion manifold learning: The motion manifold model consists of two neural networks, an encoder $g_\theta : \mathcal{X} \rightarrow \mathcal{Z}$ and a decoder $f_\theta : \mathcal{Z} \rightarrow \mathcal{X}$, where $\mathcal{Z} = \mathbb{R}^m$ is the latent space. Given a suitable distance metric $d(\cdot, \cdot)$ in \mathcal{X} , we train an autoencoder as follows:

$$\min_{\theta} \frac{1}{N} \sum_{i=1}^N d^2(x_i, f_\theta(g_\theta(x_i))) + \eta \|g_\theta(x_i)\|^2 + \delta \mathcal{E}(f_\theta, g_\theta), \quad (2)$$

where η, δ are some positive scalars. The second term penalizes the norm of latent values to prevent them from diverging excessively far from the origin. The third term is an expected energy of the decoded trajectories, added to ensure their smoothness, which is defined as follows:

$$\mathcal{E}(f_\theta, g_\theta) := \mathbb{E}_z \left[\frac{1}{T-1} \sum_{t=1}^{T-1} \left\| \frac{f_\theta^{t+1}(z) - f_\theta^t(z)}{dt} \right\|^2 \right], \quad (3)$$

where $z = \alpha g_\theta(x_i) + (1 - \alpha) g_\theta(x_j)$ and $\alpha \sim \mathcal{U}[-0.4, 1.4]$ and x_i, x_j are sampled from the dataset. Then the trained decoder parametrizes an m -dimensional motion manifold embedded in the trajectory space (see section 3.1).

Robust text-conditional latent flow learning: The latent space flow-based model consists of two neural networks. One is a text embedding neural network h_θ that maps $c \mapsto \tau = h_\theta(c) \in \mathcal{T}$, where $\mathcal{T} = \mathbb{R}^p$ is called a text embedding space. The other is a neural network vector field $v(\cdot; \theta)$ in the latent space that maps $(t, z, \tau) \mapsto v_t(z, \tau; \theta) \in T_z \mathcal{Z}$, where $T_z \mathcal{Z}$ is the tangent space of \mathcal{Z} at z . We train these two networks simultaneously with the following *regularized* flow matching loss:

$$\min_{\theta} \frac{1}{NM} \sum_{i=1}^N \sum_{j=1}^M \left(\mathbb{E}_{t,z} [\|v_t(z, h_\theta(c_{ij}); \theta) - u_t(z|z_i)\|^2] + \frac{\gamma}{K} \sum_{k=1}^K \|h_\theta(c_{ij}) - h_\theta(\tilde{c}_{ij}^k)\|^2 \right). \quad (4)$$

In the expectation of the first term, t, z are sampled from $\mathcal{U}[0, 1], p_t(z|z_i)$, respectively, and $p_t(z|z_i)$ is defined as the OT Gaussian path and $u_t(z|z_i)$ is derived from it (see section 3.2). The second

term, multiplied by a positive weight γ , is added to ensure robustness against diverse text variations. Here, \tilde{c}_{ij}^k are Sentence-BERT encoding vectors that have meanings similar to those of c_{ij} , which are generated via the Large Language Model ChatGPT.

Using the trained text embedding model h_θ , vector field v_θ , and decoder f_θ , we can generate, given a free-form text input, diverse trajectories by the following procedure (see Figure 2): (i) encode the text input using the Sentence-BERT to c , (ii) embed c to a text embedding vector $\tau = h_\theta(c)$, (iii) solve an ODE $\dot{z} = v_t(z, \tau; \theta)$ from $t = 0$ to $t = 1$ with initial samples $z_0 \sim p_0(z) = \mathcal{N}(z|0, I)$ and obtain $z_1 \in \mathcal{Z}$, and (iv) map the ODE solutions z_1 to trajectories $x = f_\theta(z_1)$. We refer our entire framework to as *Motion Manifold Flow Primitives (MMFP)*.

5 Experiments

In this section, we evaluate our method, the MMFP, mainly compared to (i) Denoising Diffusion Probabilistic Models (DDPM) [9] trained in the trajectory space \mathcal{X} – when \mathcal{X} is $SE(3)^T$, we train DDPM in local coordinates –, (ii) Flow Matching (FM) [12] trained in the trajectory space \mathcal{X} – when \mathcal{X} is $SE(3)^T$, we use the Riemannian Flow Matching (RFM) [13] –, (iii) Task-Conditional Variational Autoencoder (TCVAE) with Gaussian prior [16], and (iv) Motion Manifold Primitives with Gaussian mixture prior (MMP) [15]. MMFP trained without the regularization term (i.e., the second term in (4)) in the latent flow learning will be denoted by MMFP w/o reg. We compare models for 6-DoF $SE(3)$ pouring trajectory generation and 7-DoF robot arm waving motion generation tasks. Training details are available in the Supplementary Material.

Evaluation metrics: To measure the similarity between the generated trajectories given a text input and demonstration trajectories annotated with that text, we use the Maximum Mean Discrepancy (MMD) [59]; the lower, the better. Texts are annotated to each trajectory in three different levels (e.g. see Figure 3 *Left*) and the MMD metrics are measured separately for each text input, and then averaged across text descriptions at the same level. To evaluate the robustness to text variations, we also report robust MMD metrics. These are computed with unseen unbiased text inputs generated by ChatGPT. Lastly, to evaluate whether the model generates accurate motions that perform the task described in the given text, we train a trajectory classifier, and use it to report the motion accuracy; the higher, the better. More details are available in the Supplementary Material.

5.1 Text-based pouring motion generation

In this section, we train text-based pouring motion generation models, where the dataset is obtained from the human demonstration videos. The demonstrator is instructed to pour water or wine in five different pouring directions (i.e., from the very left, left, center, right, and very right side). When pouring wine, the demonstrator is instructed to turn the wrist clockwise at the end. From ten videos, we extract $SE(3)$ trajectories of the bottles, and the trajectory lengths are pre-processed so that $T = 480$. For each trajectory $x_i \in \mathcal{X}$, we give three text annotations, i.e., $\{c_{ij}\}_{j=1}^M$ for $M = 3$ as shown in Figure 3 (*Left*).

Table 1 shows MMD, robust MMD, and Accuracy; our MMFP only shows good scores in all metrics. We note that the regularization in MMFP significantly improves the level 3 robust MMD metric.

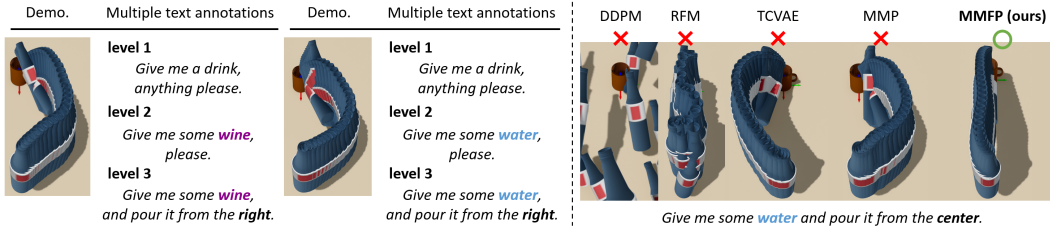


Figure 3: *Left*: Example demonstration trajectories, each of which is annotated with three different level texts. *Right*: Generated pouring trajectories by RFM, TCVAE, MMP and MMFP.

	MMD (\downarrow)			robust MMD (\downarrow)			Accuracy (\uparrow)		
	level 1	level 2	level 3	level 1	level 2	level 3	pouring style	pouring direction	both
DDPM [9]	0.398	0.484	1.306	0.400	0.486	1.304	50.5	20.0	10.2
RFM [13]	0.411	0.431	0.778	0.413	0.425	1.127	87.0	36.4	30.8
TCVAE [16]	0.117	0.211	0.824	0.131	0.191	1.041	52.0	25.4	15.3
MMP [15]	0.045	0.115	0.950	0.055	0.112	0.970	47.5	19.6	9.3
MMFP w/o reg (ours)	0.055	0.114	0.009	0.056	0.097	0.096	98.5	93.2	99.9
MMFP (ours)	0.042	0.093	0.007	0.052	0.094	0.016	99.0	92.6	99.9

Table 1: The MMD and robust MMD metrics and the accuracy (%) for pouring motion generation.

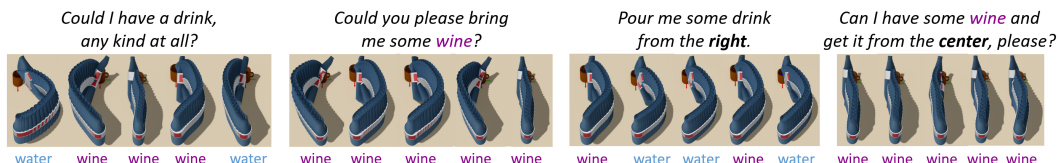


Figure 4: A variety of accurate trajectories generated by MMFP given unbiased text inputs.

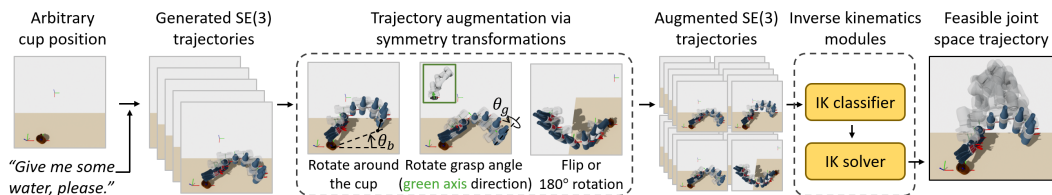


Figure 5: The procedure of a feasible joint space trajectory generation.

The DDPM and RFM overall produce very poor MMD results. As shown in Figure 3 (Right), the trajectory generated by DDPM does not even converge near the cup and that of RFM is very jerky. TCVAE and MMP, both adopting the motion manifold hypothesis, produce motions of reasonable quality. Nevertheless, they exhibit a limitation in understanding level 3 text descriptions, particularly regarding pouring directions. Examples illustrating this limitation can be observed in Figure 3 (Right), where they fail in pouring from accurate directions. Lastly, Figure 4 shows a variety of accurately generated motions by MMFP given unbiased user text inputs not seen during training.

Now, when provided with SE(3) trajectories of a bottle sampled using our MMFP, we propose a method to quickly find feasible joint space trajectories for an arbitrary 2D position of the cup; see Figure 5 for the overview. To begin, for a given SE(3) trajectory of a bottle, we leverage symmetries in the pouring task to augment it into diverse SE(3) trajectories. This augmentation involves three types of transformations, as illustrated in Figure 5 (Trajectory augmentation via symmetry transformations): (1) rotation of the bottle around the cup axis by $\theta_b \in [-30^\circ, 30^\circ]$, (2) rotation of the bottle frame by $\theta_g \in [-60^\circ, 60^\circ]$ that changes the grasping pose – where the robot reaches and grasps the bottle in the green axis direction –, and (3) flipping the bottle with respect to the cup (i.e., rotating it by 180°). Each generated trajectory undergoes a total of $50 = 5 \times 5 \times 2$ transformations. This involves discretizing $[-30^\circ, 30^\circ]$ and $[-60^\circ, 60^\circ]$ into

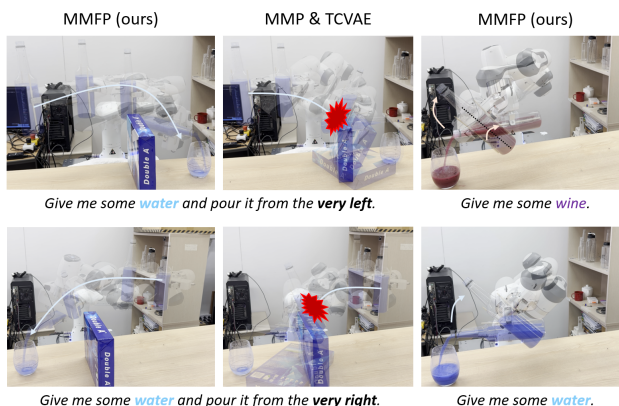


Figure 6: Real robot pouring motion generation results.

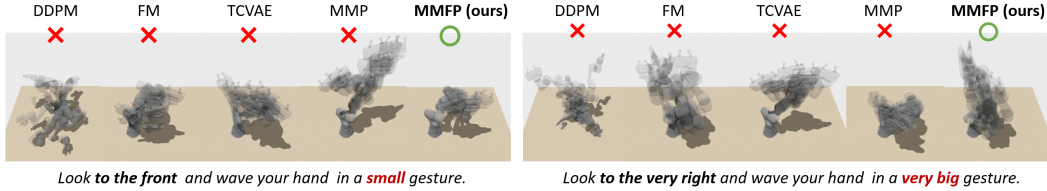


Figure 8: Generated waving trajectories by DDPM, FM, TCVAE, MMP and MMFP.

5 points with equal-size intervals for θ_b and θ_g , respectively. Additionally, multiples of 2 are considered for flipping. We generate five trajectories for a single text input, resulting in a total of 250 candidate SE(3) trajectories that require verification for the existence of an IK solution. We train and use a neural IK classifier to boost the speed of finding feasible joint trajectories. An example SE(3) trajectory whose IK solution exists is shown in Figure 5 (Feasible joint space trajectory); other examples can be found in the Supplementary Material.

We conduct real robot experiments with two scenarios. First, we put an obstacle blocking the middle path, and ask the robot “Give me some water, and pour it from the very left/right side.”, so that it pours water while turning away to avoid collision; see Figure 6 (Upper). Second, we ask the robot “Give me some wine/water.”, and see if it shows clockwise rotation behavior of the bottle at the end of the pouring; see Figure 6 (Lower). We generate three joint space trajectories for each text input, and measure the success rates. Success is judged by human observation. Table 2 shows the success rates². MMFP outperforms TCVAE and MMP in all experiments. We note that, in EXP 3, the success rate of MMFP is 2/3. Judging by human observation, one trajectory is somewhat ambiguous to determine whether the robot is pouring water or pouring wine. Figure 6 shows examples where MMFP successfully avoids the obstacle and shows the correct pouring style.

	TCVAE	MMP	MMFP (ours)
EXP 1 (very left side)	0/3	1/3	3/3
EXP 2 (very right side)	0/3	2/3	3/3
EXP 3 (wine)	1/3	1/3	2/3
EXP 4 (water)	0/3	1/3	3/3

Table 2: Real robot success rates given language guidance.

5.2 Text-based 7-DoF waving motion generation

In this section, we train text-based 7-DoF waving motion generation models, where the dataset is obtained from human demonstrations. The demonstrator is instructed to hold and move the robot arm so that the robot arm mimics waving motions in five different viewing directions (i.e., very left, left, front, right, and very right) and in three different styles (i.e., very big, big, small). We extract

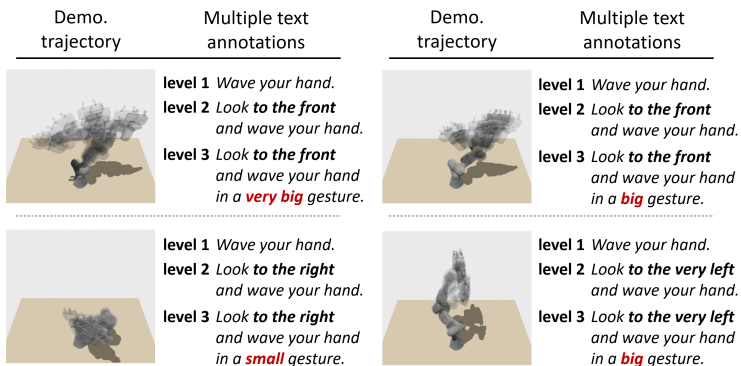


Figure 7: Example 7-DoF demonstration trajectories, each of which is assigned with three different text labels.

7-DoF joint space trajectories, and the trajectory lengths are pre-processed to ensure $T = 720$. We encode two motions for each setting, resulting in a total of $N = 30$ trajectories. For each trajectory $x_i \in \mathcal{X}$, we provide three text annotations, denoted by $\{c_{ij}\}_{j=1}^M$ for $M = 3$, as shown in Figure 7.

²Trajectories from DDPM and RFM are too jerky to be deployed in the real robot.

	MMD (\downarrow)			robust MMD (\downarrow)			Accuracy (\uparrow)		
	level 1	level 2	level 3	level 1	level 2	level 3	waving direction	waving style	both
DDPM [9]	0.425	0.542	0.831	0.427	0.542	0.831	18.4	29.3	4.1
FM [12]	0.211	0.368	0.646	0.215	0.384	0.671	99.6	88.7	91.1
TCVAE [16]	0.269	0.581	0.833	0.294	0.606	0.865	25.6	57.3	10.7
MMP [15]	0.013	0.369	0.772	0.016	0.355	0.750	19.2	30.7	6.5
MMFP w/o reg (ours)	0.020	0.037	0.006	0.024	0.046	0.021	99.8	98.7	99.7
MMFP (ours)	0.016	0.040	0.004	0.022	0.040	0.005	100	97.7	100

Table 3: The MMD and robust MMD metrics and the accuracy (%) for waving motion generation.

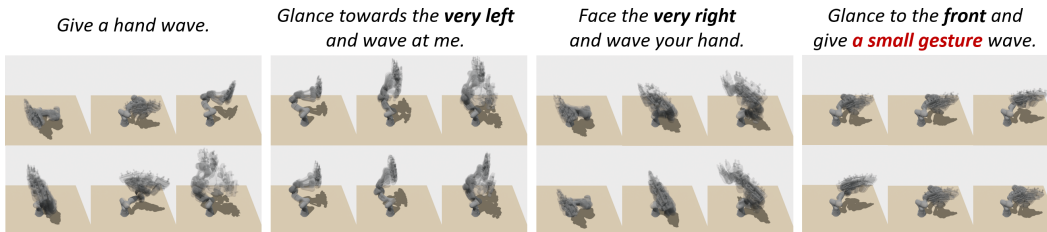


Figure 9: A variety of accurate trajectories generated by MMFP given unbiased text inputs.

Table 3 shows MMD, robust MMD, and Accuracy; MMFP again only shows good scores in all metrics. We also note that the regularization in MMFP significantly improves the level 3 robust MMD metric. The DDPM and FM again produce very poor MMD results, and their generated trajectories generated, as shown in Figure 8, are very jerky. TCVAE and MMP, both adopting the motion manifold hypothesis, produce motions of reasonable quality. Nevertheless, they exhibit a limitation in understanding detailed text instructions, both level 2 and level 3. Examples illustrating this limitation can be observed in Figure 8, where they fail in waving to accurate directions and with accurate styles. Lastly, Figure 9 shows a variety of accurately generated motions by MMFP, given unbiased user text inputs not seen during training. Some real robot waving motion generation results by our MMFP are visualized in Figure 10.

6 Limitation

Learned motion manifolds effectively interpolate given demonstration trajectories, but struggle to extrapolate and generate more varied motions. For instance, in our pouring task, the demonstrations are restricted to turning left or right, so the model is not able to produce motions turning upwards or downwards. Collecting more trajectory data could solve this problem, but data collection is costly. Ideally, a solution that bypasses the need for additional data would be preferable.

7 Conclusion

The Motion Manifold Flow Primitive (MMFP) framework presented in this paper combines motion manifolds and latent space flows, and allows for the construction of models that can learn complex text-conditional distributions from a small number of trajectory data, each labeled with multiple text annotations. Proper regularization has been designed to ensure the smoothness of the generated trajectories and robustness to unstructured text variations. Our experimental results demonstrate accurate motion generation even for unseen text inputs, which contrasts with existing manifold-based methods such as TCVAE and MMP, and trajectory space diffusion and flow-based models.



Figure 10: Real robot waving motion generation by MMFP.

References

- [1] R. Rombach, A. Blattmann, D. Lorenz, P. Esser, and B. Ommer. High-resolution image synthesis with latent diffusion models. In *Proceedings of the IEEE/CVF conference on computer vision and pattern recognition*, pages 10684–10695, 2022.
- [2] C. Saharia, W. Chan, S. Saxena, L. Li, J. Whang, E. L. Denton, K. Ghasemipour, R. Gontijo Lopes, B. Karagol Ayan, T. Salimans, et al. Photorealistic text-to-image diffusion models with deep language understanding. *Advances in Neural Information Processing Systems*, 35: 36479–36494, 2022.
- [3] B. Poole, A. Jain, J. T. Barron, and B. Mildenhall. Dreamfusion: Text-to-3d using 2d diffusion. *arXiv preprint arXiv:2209.14988*, 2022.
- [4] C.-H. Lin, J. Gao, L. Tang, T. Takikawa, X. Zeng, X. Huang, K. Kreis, S. Fidler, M.-Y. Liu, and T.-Y. Lin. Magic3d: High-resolution text-to-3d content creation. In *Proceedings of the IEEE/CVF Conference on Computer Vision and Pattern Recognition*, pages 300–309, 2023.
- [5] M. Zhang, Z. Cai, L. Pan, F. Hong, X. Guo, L. Yang, and Z. Liu. Motiondiffuse: Text-driven human motion generation with diffusion model. *arXiv preprint arXiv:2208.15001*, 2022.
- [6] J. Kim, J. Kim, and S. Choi. Flame: Free-form language-based motion synthesis & editing. In *Proceedings of the AAAI Conference on Artificial Intelligence*, volume 37, pages 8255–8263, 2023.
- [7] J. Devlin, M.-W. Chang, K. Lee, and K. Toutanova. Bert: Pre-training of deep bidirectional transformers for language understanding. *arXiv preprint arXiv:1810.04805*, 2018.
- [8] Y. Liu, M. Ott, N. Goyal, J. Du, M. Joshi, D. Chen, O. Levy, M. Lewis, L. Zettlemoyer, and V. Stoyanov. Roberta: A robustly optimized bert pretraining approach. *arXiv preprint arXiv:1907.11692*, 2019.
- [9] J. Ho, A. Jain, and P. Abbeel. Denoising diffusion probabilistic models. *Advances in neural information processing systems*, 33:6840–6851, 2020.
- [10] J. Song, C. Meng, and S. Ermon. Denoising diffusion implicit models. *arXiv preprint arXiv:2010.02502*, 2020.
- [11] Y. Song, J. Sohl-Dickstein, D. P. Kingma, A. Kumar, S. Ermon, and B. Poole. Score-based generative modeling through stochastic differential equations. *arXiv preprint arXiv:2011.13456*, 2020.
- [12] Y. Lipman, R. T. Chen, H. Ben-Hamu, M. Nickel, and M. Le. Flow matching for generative modeling. *arXiv preprint arXiv:2210.02747*, 2022.
- [13] R. T. Chen and Y. Lipman. Riemannian flow matching on general geometries. *arXiv preprint arXiv:2302.03660*, 2023.
- [14] A. Tong, N. Malkin, G. Huguet, Y. Zhang, J. Rector-Brooks, K. Fatras, G. Wolf, and Y. Bengio. Conditional flow matching: Simulation-free dynamic optimal transport. *arXiv preprint arXiv:2302.00482*, 2023.
- [15] B. Lee, Y. Lee, S. Kim, M. Son, and F. C. Park. Equivariant motion manifold primitives. In *Conference on Robot Learning*, pages 1199–1221. PMLR, 2023.
- [16] M. Noseworthy, R. Paul, S. Roy, D. Park, and N. Roy. Task-conditioned variational autoencoders for learning movement primitives. In *Conference on robot learning*, pages 933–944. PMLR, 2020.
- [17] M. Saveriano, F. J. Abu-Dakka, A. Kramberger, and L. Peternel. Dynamic movement primitives in robotics: A tutorial survey. *arXiv preprint arXiv:2102.03861*, 2021.

- [18] A. J. Ijspeert, J. Nakanishi, H. Hoffmann, P. Pastor, and S. Schaal. Dynamical movement primitives: learning attractor models for motor behaviors. *Neural computation*, 25(2):328–373, 2013.
- [19] A. J. Ijspeert, J. Nakanishi, and S. Schaal. Trajectory formation for imitation with nonlinear dynamical systems. In *Proceedings 2001 IEEE/RSJ International Conference on Intelligent Robots and Systems. Expanding the Societal Role of Robotics in the the Next Millennium (Cat. No. 01CH37180)*, volume 2, pages 752–757. IEEE, 2001.
- [20] A. J. Ijspeert, J. Nakanishi, and S. Schaal. Learning rhythmic movements by demonstration using nonlinear oscillators. In *Proceedings of the ieee/rsj int. conference on intelligent robots and systems (iros2002)*, number CONF, pages 958–963, 2002.
- [21] S. Schaal, P. Mohajerin, and A. Ijspeert. Dynamics systems vs. optimal control—a unifying view. *Progress in brain research*, 165:425–445, 2007.
- [22] A. Pervez, A. Ali, J.-H. Ryu, and D. Lee. Novel learning from demonstration approach for repetitive teleoperation tasks. In *2017 IEEE World Haptics Conference (WHC)*, pages 60–65. IEEE, 2017.
- [23] Y. Fanger, J. Umlauf, and S. Hirche. Gaussian processes for dynamic movement primitives with application in knowledge-based cooperation. In *2016 IEEE/RSJ International Conference on Intelligent Robots and Systems (IROS)*, pages 3913–3919. IEEE, 2016.
- [24] J. Umlauf, Y. Fanger, and S. Hirche. Bayesian uncertainty modeling for programming by demonstration. In *2017 IEEE International Conference on Robotics and Automation (ICRA)*, pages 6428–6434. IEEE, 2017.
- [25] A. Pervez, Y. Mao, and D. Lee. Learning deep movement primitives using convolutional neural networks. In *2017 IEEE-RAS 17th international conference on humanoid robotics (Humanoids)*, pages 191–197. IEEE, 2017.
- [26] S. Bahl, M. Mukadam, A. Gupta, and D. Pathak. Neural dynamic policies for end-to-end sensorimotor learning. *Advances in Neural Information Processing Systems*, 33:5058–5069, 2020.
- [27] S. M. Khansari-Zadeh and A. Billard. Learning stable nonlinear dynamical systems with gaussian mixture models. *IEEE Transactions on Robotics*, 27(5):943–957, 2011.
- [28] K. Neumann, A. Lemme, and J. J. Steil. Neural learning of stable dynamical systems based on data-driven lyapunov candidates. In *2013 IEEE/RSJ International Conference on Intelligent Robots and Systems*, pages 1216–1222. IEEE, 2013.
- [29] S. M. Khansari-Zadeh and A. Billard. Learning control lyapunov function to ensure stability of dynamical system-based robot reaching motions. *Robotics and Autonomous Systems*, 62(6): 752–765, 2014.
- [30] A. Lemme, K. Neumann, R. F. Reinhart, and J. J. Steil. Neural learning of vector fields for encoding stable dynamical systems. *Neurocomputing*, 141:3–14, 2014.
- [31] K. Neumann and J. J. Steil. Learning robot motions with stable dynamical systems under diffeomorphic transformations. *Robotics and Autonomous Systems*, 70:1–15, 2015.
- [32] C. Blocher, M. Saveriano, and D. Lee. Learning stable dynamical systems using contraction theory. In *2017 14th International Conference on Ubiquitous Robots and Ambient Intelligence (URAI)*, pages 124–129. IEEE, 2017.
- [33] N. Figueroa and A. Billard. A physically-consistent bayesian non-parametric mixture model for dynamical system learning. In *CoRL*, pages 927–946, 2018.

- [34] V. Sindhvani, S. Tu, and M. Khansari. Learning contracting vector fields for stable imitation learning. *arXiv preprint arXiv:1804.04878*, 2018.
- [35] J. Z. Kolter and G. Manek. Learning stable deep dynamics models. *Advances in neural information processing systems*, 32, 2019.
- [36] S. Calinon. A tutorial on task-parameterized movement learning and retrieval. *Intelligent service robotics*, 9:1–29, 2016.
- [37] D. A. Duque, F. A. Prieto, and J. G. Hoyos. Trajectory generation for robotic assembly operations using learning by demonstration. *Robotics and Computer-Integrated Manufacturing*, 57: 292–302, 2019.
- [38] C. Yang, C. Chen, N. Wang, Z. Ju, J. Fu, and M. Wang. Biologically inspired motion modeling and neural control for robot learning from demonstrations. *IEEE Transactions on Cognitive and Developmental Systems*, 11(2):281–291, 2018.
- [39] S. Chernova and M. Veloso. Confidence-based policy learning from demonstration using gaussian mixture models. In *Proceedings of the 6th international joint conference on Autonomous agents and multiagent systems*, pages 1–8, 2007.
- [40] A. Paraschos, C. Daniel, J. R. Peters, and G. Neumann. Probabilistic movement primitives. *Advances in neural information processing systems*, 26, 2013.
- [41] N. Ruiz, Y. Li, V. Jampani, Y. Pritch, M. Rubinstein, and K. Aberman. Dreambooth: Fine tuning text-to-image diffusion models for subject-driven generation. In *Proceedings of the IEEE/CVF Conference on Computer Vision and Pattern Recognition*, pages 22500–22510, 2023.
- [42] C. Zhang, C. Zhang, M. Zhang, and I. S. Kweon. Text-to-image diffusion model in generative ai: A survey. *arXiv preprint arXiv:2303.07909*, 2023.
- [43] Y. Balaji, S. Nah, X. Huang, A. Vahdat, J. Song, K. Kreis, M. Aittala, T. Aila, S. Laine, B. Catanzaro, et al. ediffi: Text-to-image diffusion models with an ensemble of expert denoisers. *arXiv preprint arXiv:2211.01324*, 2022.
- [44] G. Tevet, S. Raab, B. Gordon, Y. Shafir, D. Cohen-Or, and A. H. Bermano. Human motion diffusion model. *arXiv preprint arXiv:2209.14916*, 2022.
- [45] L. Wang, N. Yang, X. Huang, B. Jiao, L. Yang, D. Jiang, R. Majumder, and F. Wei. Text embeddings by weakly-supervised contrastive pre-training. *arXiv preprint arXiv:2212.03533*, 2022.
- [46] Z. Li, X. Zhang, Y. Zhang, D. Long, P. Xie, and M. Zhang. Towards general text embeddings with multi-stage contrastive learning, 2023.
- [47] I. Beltagy, M. E. Peters, and A. Cohan. Longformer: The long-document transformer. *arXiv:2004.05150*, 2020.
- [48] A. Padalkar, A. Pooley, A. Jain, A. Bewley, A. Herzog, A. Irpan, A. Khazatsky, A. Rai, A. Singh, A. Brohan, et al. Open x-embodiment: Robotic learning datasets and rt-x models. *arXiv preprint arXiv:2310.08864*, 2023.
- [49] A. Brohan, N. Brown, J. Carbajal, Y. Chebotar, J. Dabis, C. Finn, K. Gopalakrishnan, K. Hausman, A. Herzog, J. Hsu, et al. Rt-1: Robotics transformer for real-world control at scale. *arXiv preprint arXiv:2212.06817*, 2022.
- [50] G. Arvanitidis, L. K. Hansen, and S. Hauberg. Latent space oddity: on the curvature of deep generative models. *arXiv preprint arXiv:1710.11379*, 2017.

- [51] Y. Lee, H. Kwon, and F. Park. Neighborhood reconstructing autoencoders. *Advances in Neural Information Processing Systems*, 34:536–546, 2021.
- [52] Y. Lee, S. Kim, J. Choi, and F. Park. A statistical manifold framework for point cloud data. In *International Conference on Machine Learning*, pages 12378–12402. PMLR, 2022.
- [53] Y. Lee, S. Yoon, M. Son, and F. C. Park. Regularized autoencoders for isometric representation learning. In *International Conference on Learning Representations*, 2022.
- [54] C. Jang, Y. Lee, Y.-K. Noh, and F. C. Park. Geometrically regularized autoencoders for non-euclidean data. In *The Eleventh International Conference on Learning Representations*.
- [55] Y. Lee. A geometric perspective on autoencoders. *arXiv preprint arXiv:2309.08247*, 2023.
- [56] Y. Lee and F. C. Park. On explicit curvature regularization in deep generative models. In *Topological, Algebraic and Geometric Learning Workshops 2023*, pages 505–518. PMLR, 2023.
- [57] R. T. Chen, Y. Rubanova, J. Bettencourt, and D. K. Duvenaud. Neural ordinary differential equations. *Advances in neural information processing systems*, 31, 2018.
- [58] N. Reimers and I. Gurevych. Sentence-bert: Sentence embeddings using siamese bert-networks. In *Proceedings of the 2019 Conference on Empirical Methods in Natural Language Processing*. Association for Computational Linguistics, 11 2019. URL <https://arxiv.org/abs/1908.10084>.
- [59] A. Gretton, K. M. Borgwardt, M. J. Rasch, B. Schölkopf, and A. Smola. A kernel two-sample test. *The Journal of Machine Learning Research*, 13(1):723–773, 2012.